



Deposited via The University of Sheffield.

White Rose Research Online URL for this paper:

<https://eprints.whiterose.ac.uk/id/eprint/135655/>

Version: Accepted Version

Article:

Ahmad, M.I.M., Curiel-Sosa, J.L., Arun, S. et al. (2019) An enhanced void-crack based Rousselier damage model for ductile fracture with the XFEM. *International Journal of Damage Mechanics*, 28 (6). pp. 943-969. ISSN: 1056-7895

<https://doi.org/10.1177/1056789518802624>

© 2018 The Authors. This is an author produced version of a paper subsequently published in *International Journal of Damage Mechanics*. Uploaded in accordance with the publisher's self-archiving policy. Article available under the terms of the CC-BY-NC-ND licence (<https://creativecommons.org/licenses/by-nc-nd/4.0/>).

Reuse

This article is distributed under the terms of the Creative Commons Attribution-NonCommercial-NoDerivs (CC BY-NC-ND) licence. This licence only allows you to download this work and share it with others as long as you credit the authors, but you can't change the article in any way or use it commercially. More information and the full terms of the licence here: <https://creativecommons.org/licenses/>

Takedown

If you consider content in White Rose Research Online to be in breach of UK law, please notify us by emailing eprints@whiterose.ac.uk including the URL of the record and the reason for the withdrawal request.

An Enhanced Void-Crack based Rousselier Damage Model for Ductile Fracture with the XFEM

Journal:	<i>International Journal of Damage Mechanics</i>
Manuscript ID	IJDM-18-067.R2
Manuscript Type:	Original Manuscript
Date Submitted by the Author:	24-Jul-2018
Complete List of Authors:	MEOR AHMAD, MEOR IQRAM; University of Sheffield Department of Mechanical Engineering, Curiel Sosa, Jose Luis; University of Sheffield, Mechanical Engineering Rongong, Jem; University of Sheffield Department of Mechanical Engineering Arun, Sutham; School of Mechanical Engineering University of Phayao, Thailand
Keywords:	Ductile fracture, Rousselier, XFEM, crack, void damage
Abstract:	This work presents a modelling strategy for ductile fracture materials by implementing the Rousselier damage model with the extended finite element method (XFEM). The implicit integration scheme and consistent tangent modulus (CTM) based on a radial return mapping algorithm for this constitutive model are developed by the user-defined material subroutine UMAT in ABAQUS/ Standard. To enhance the modelling of the crack development in the materials, the XFEM is used that allows modelling of arbitrary discontinuities, where the mesh does not have to be aligned with the boundaries of material interfaces. This modelling strategy, so-called Rousselier-UMAT-XFEM (RuX) model is proposed to connect both concepts, which gives an advantage in predicting the material behaviour of ductile material in terms of voids and crack relation. This is the first contribution where XFEM is used in ductile fracture analysis for micromechanical damage problems. The results indicate that the RuX model is a promising technique for predicting the void volume fraction damage and crack extension in ductile material, which shows a good agreement in terms of stress-strain and force-displacement relationships.

An Enhanced Void-Crack based Rousselier Damage Model for Ductile Fracture with the XFEM

M.I.M. Ahmad^{a,b,c,*}, J.L. Curiel-Sosa^{a,b}, S. Arun^d, J.A. Rongong^a

^a*Department of Mechanical Engineering, The University of Sheffield, Sir Frederick Mappin Building, Mappin Street, S1 3JD Sheffield, United Kingdom*

^b*Computer-Aided Aerospace and Mechanical Engineering Research Group (CA²M), University of Sheffield, Sheffield, UK*

^c*Department of Mechanical and Materials Engineering, Faculty of Engineering and Build Environments, University Kebangsaan Malaysia, 43600 UKM Bangi, Selangor, Malaysia*

^d*School of Mechanical Engineering, University of Phayao, Phayao, Thailand*

Abstract

This work presents a modelling strategy for ductile fracture materials by implementing the Rousselier damage model with the extended finite element method (XFEM). The implicit integration scheme and consistent tangent modulus (CTM) based on a radial return mapping algorithm for this constitutive model are developed by the user-defined material subroutine UMAT in ABAQUS/ Standard. To enhance the modelling of the crack development in the materials, the XFEM is used that allows modelling of arbitrary discontinuities, where the mesh does not have to be aligned with the boundaries of material interfaces. This modelling strategy, so-called Rousselier-UMAT-XFEM (RuX) model is proposed to connect both concepts, which gives an advantage in predicting the material behaviour of ductile material in terms of voids and crack relation. This is the first contribution where XFEM is used in ductile fracture analysis for micromechanical damage problems. The results indicate that the RuX model is a promising technique for predicting the void volume fraction damage and crack extension in ductile material, which shows a good agreement in terms of stress-strain and force-displacement relationships.

Keywords:

Ductile fracture, Rousselier, XFEM, crack, void damage.

1. Introduction

Materials and structures do not only deform plastically but are also subjected to damage [1]. The internal damage variable approach defines damage as the modification of the physical properties of materials related to irreversible growth in micro-defects [2]. Three stages occur in ductile fracture [3, 4]: firstly, voids initiate at material defects; next, the voids enlarge where the stress triaxiality is large due to significant plastic deformation; finally, when the voids are large enough, they coalesce to form microcracks from which a macroscopic crack develops leading to macroscopic failure.

By considering the ductile damage caused by plastic void growth, a micromechanics based model was developed by Gurson [5] in 1977 and phenomenologically extended in 1984 by Tvergaard and Needleman (the so-called as GTN model) [6]. Rousselier [7, 9] then extended this model further by characterizing the thermodynamic state with the hardening and softening of the material into the internal variables in the framework of the plastic potential. There has been considerable research interest in the constitutive

*Corresponding author

Email address: mimeorahmad1@sheffield.ac.uk (M.I.M. Ahmad)

1 relations of void growth and damage for the modelling of ductile fracture. For example, Batische et al.
2 [10] investigated the ductile fracture of A508 Cl 3 steel in different heat conditions based on the local
3 approach of fracture. In a separate study, Guo J. et al. [11] studied the ductile fracture of Al-alloy 5052
4 by implementing the modified Rousselier model for both tension and shear failure in a numerical and
5 experimental investigation. This was next followed by modelling ductile fracture over the entire range
6 of stress triaxiality based on classical void growth and the Mohr-Coulomb model for 6260 thin-walled
7 aluminium extrusion material [12].

8 For the extended study, it is interesting to explore the relationship of the knowledge of void ductile
9 damage with the crack development of the material [13]. The advanced numerical technique called
10 the Extended Finite Element Method (XFEM) is employed to model crack development, under the
11 assumptions of linear elastic fracture mechanics [14]. Since its introduction, XFEM has been developed
12 and used in many applications [15]. For example dynamic analysis of a stationary crack [16], failure
13 analysis of fibre metal laminates [17], modelling of quasi-static crack growth [18], and the analysis of
14 ductile damage model (Lemaitre model) for crack initiation and propagation [19].

15 The aim of this paper is to develop the connection between the micromechanical constitutive damage
16 model and crack development, in which the Rousselier-UMAT-XFEM (RuX) model is proposed and
17 used to represent an extensive analysis of ductile damage with a crack in the material. Indeed, this is
18 an exciting new achievement by implementing the XFEM solution in the constitutive Rousselier damage
19 model, which gives benefit in terms of the mathematical formulation to predict the void damage together
20 with the crack development of the ductile materials.

21 Accordingly, this paper is organized into five sections. An overview of the RuX model is given in
22 Section 2. Section 3 describes numerical frameworks, which is then followed by Section 4, which presents
23 the results and discussion of the study. Finally, Section 5 provides the concluding remarks of this paper.
24
25
26
27
28
29
30
31
32
33
34
35
36
37
38
39
40
41
42
43
44
45
46
47
48
49
50
51
52
53
54
55
56
57
58
59
60

2. Overview of the RuX model

The RuX model solution has been proposed to predict the micromechanical damage of the material with the existing crack development. The RuX model is a combined term of the Rousselier model (constitutive damage model), UMAT subroutine (interface user-defined material) and XFEM solution (crack development). Fig. 1 illustrates the flow-diagram, displaying the steps involved in the model.

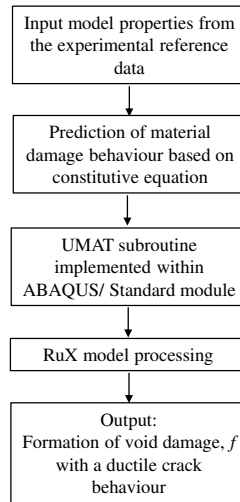


Figure 1: The flow diagram of RuX model

The Rousselier model was implemented using an Abaqus UMAT subroutine to describe material damage [29]. In the subroutine, the integration scheme utilizing the radial return algorithm and implicit solution method are formulated in the finite element method, which is explained in the next section. Then, to introduce the crack development in the material, the XFEM solution is proposed where the crack initiation and evolution based on the damage of traction-separation law and displacement/ energy release rate criterion are selected for characterizing the crack behaviour.

3. Numerical frameworks

3.1. Rousselier's Damage Model in UMAT Subroutines

The Rousselier model is a pressure-dependent plasticity model, which was developed based on the thermodynamics of the irreversible processes (TIP) framework [12]. In the TIP framework, the specific free energy, ψ can be defined as [7]:

$$\psi(\epsilon_{ij}^e, p, \beta) = \psi^e(\epsilon_{ij}^e) + \psi_p(\epsilon_{eq}) + \psi_\beta(\beta) \quad (1)$$

where ψ^e is elastic strain energy, ψ_p and ψ_β are the dissipated energy relating to the mechanisms of hardening and softening, respectively.

The Rousselier plastic potential is used to estimate the onset of yielding of the material point [8] which shows the presence of the void volume fraction, considered as an internal state variable in the material constitutive model. Rousselier proposed the classical plastic potential as [7, 22, 23]:

$$\phi = \frac{q}{\rho} - R(\epsilon_{eq}) + B(\beta) De^{\left(\frac{-\sigma_m}{\rho\sigma_1}\right)} \quad (2)$$

where q and σ_m are the von Mises equivalent stress and mean stress, respectively, D and σ_1 are Rousselier material parameters, ρ is a relative density, β is an internal variable describing damage and ε_{eq} is the equivalent plastic strain which represents hardening of the material. With loading, the void volume fraction evolves from the initial void volume fraction, f_0 , of the material. The void growth rate can be obtained as:

$$\dot{f} = (1 - f) \dot{\varepsilon}_{kk}^p = (1 - f) \dot{\varepsilon}_p \quad (3)$$

where $\dot{\varepsilon}_{kk}^p$ is the component of the plastic strain tensor.

By considering a material which contains a void, the relationship between the relative density, ρ , and f can be written as:

$$\rho = \left(\frac{1 - f}{1 - f_0} \right) \quad (4)$$

since the value of f_0 is very small compared to unity, Eq. (4) becomes as [24]:

$$\rho = 1 - f \quad (5)$$

However, f_0 is still be calculated in the formulation of this study, in order to see the influence of f_0 in the formation of void growth in the material. The function of $B(\beta)$ in Eq. (2) can be written in terms of the void volume fraction as:

$$B(\beta) = \sigma_1 f \quad (6)$$

By substituting Eq. (5) and Eq. (6) into Eq. (2), the Rousselier plastic potential can be written as:

$$\phi = \frac{q}{1 - f} - R(\varepsilon_{eq}) + D\sigma_1 f e^{\left(\frac{-\sigma_m}{(1-f)\sigma_1}\right)} \quad (7)$$

Next, to implement the Rousselier model as a constitutive material in the formulation, UMAT subroutine is chosen as an interface. The UMAT subroutine is the user-defined material of the ABAQUS/Standard module, which implements the implicit integration scheme to update the state of the model and the consistent tangent modulus (CTM) required for developing the mechanical constitutive model. For integration of the elastoplastic constitutive equation, the radial return algorithm [25, 26] is implemented involving two main parts; the elastic predictor part, and the plastic corrector part. The detailed formulation of the integration procedure is discussed further in the next section. Fig. 2 illustrates a full schematic flow diagram of the UMAT subroutine algorithm that is implemented in this study.

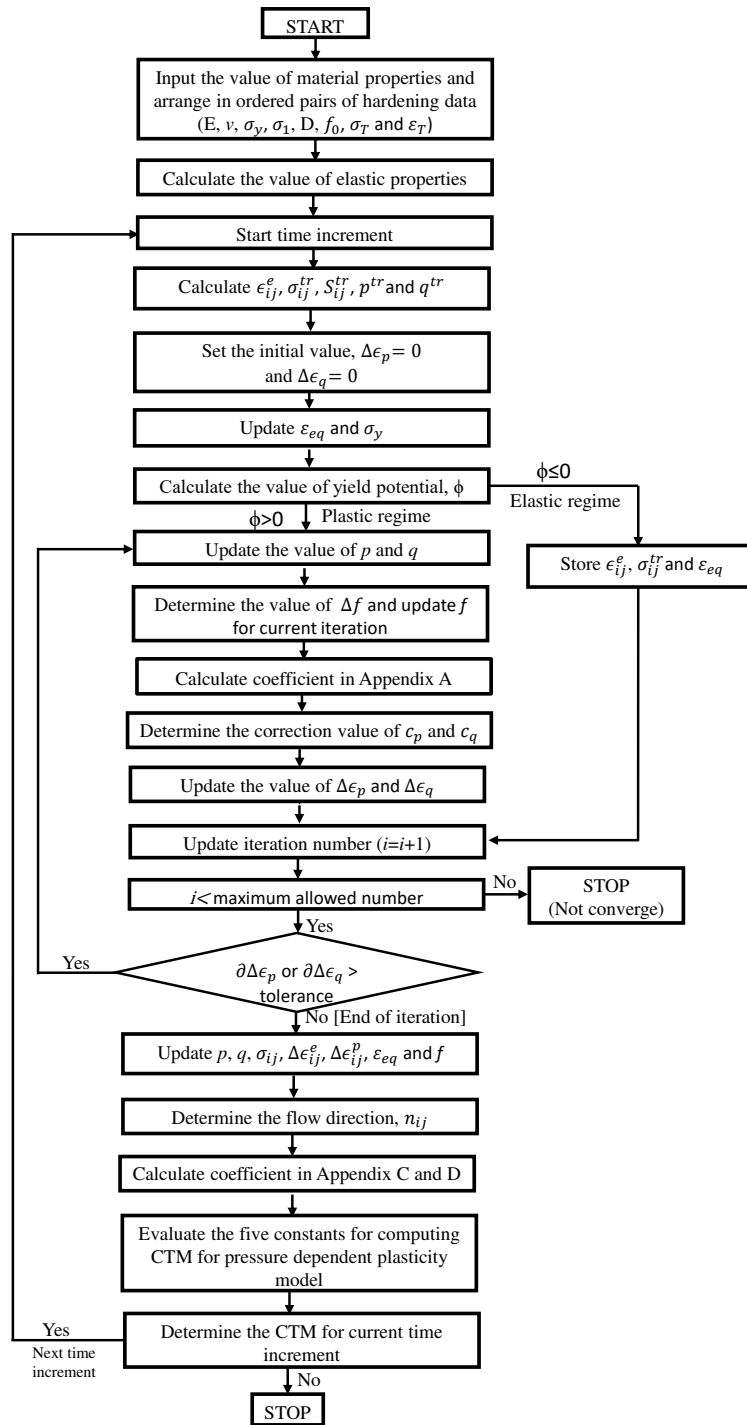


Figure 2: Schematic flow diagram of UMAT subroutine algorithm

3.2. Elastoplastic constitutive relations

The strain rate decomposition based on the deformation theory of plasticity [25] is formulated as:

$$d\epsilon_{ij} = d\epsilon_{ij}^e + d\epsilon_{ij}^p \quad (8)$$

where $d\epsilon_{ij}$, $d\epsilon_{ij}^e$ and $d\epsilon_{ij}^p$ denote the differential change in the total, elastic and plastic strain tensors respectively. Assuming small elastic strains, the Cauchy stress tensor, σ_{ij} becomes:

$$\sigma_{ij} = \frac{\partial W}{\partial \epsilon_{ij}^e} \quad (9)$$

where W is the elastic strain energy potential. For the case of isotropic elasticity, Eq. (9) becomes:

$$\sigma_{ij} = C_{ijkl}^e \epsilon_{kl}^e \quad (10)$$

$$C_{ijkl}^e = 2G\delta_{ik}\delta_{jl} + \left(K - \frac{2}{3}G\right) \delta_{ij}\delta_{kl} \quad (11)$$

where C_{ijkl}^e is a fourth order elasticity tensor, G and K are the elastic shear and bulk moduli. Next, the stress tensor in Eq. (10) can be decomposed as:

$$\sigma_{ij} = \sigma_m \delta_{ij} + S_{ij} \quad (12)$$

where δ_{ij} is the Kronecker-Delta (second order identity tensor) and S_{ij} is the deviatoric stress component.

The elastic limit of material under the combined state of stress can be substituted by a yield function which is expressed as:

$$F(p, q, H^i) = 0 \quad (13)$$

where $p = -\sigma_m$ is the hydrostatic pressure, $q = \sqrt{\frac{3}{2}S_{ij}S_{ij}}$ and $H^i, i = 1, 2, \dots$ is the internal state variable such as hardening. To establish the yield criterion, the values of yield function, F are classified as follow:

$$F < 0 : \text{Elastic deformation regime} \quad (14)$$

$$F = 0 : \text{Plastic deformation regime} \quad (15)$$

Hence, Eq. (12) becomes:

$$\sigma_{ij} = -p\delta_{ij} + \frac{2}{3}qn_{ij} \quad (16)$$

where $n_{ij} = \frac{\partial q}{\partial \sigma_{ij}} = \frac{3}{2} \frac{S_{ij}}{q}$ is the unit vector in the deviatoric space normal to the yield surface.

Moreover, to define the associated flow rule, the yield function, F and plastic potential, ϕ are taken to be identical [27], and the increment in the plastic strain tensor can be written in term of the plastic potential, ϕ as given by:

$$d\epsilon_{ij}^p = d\lambda \frac{\partial \phi}{\partial \sigma_{ij}} \quad (17)$$

where $d\lambda$ is a non-zero scalar factor of proportionality when plastic deformation occurs. The plastic strain increment in Eq. (17) can also be decoupled into volumetric, $(d\epsilon_{ij}^p)_V$ and deviatoric, $(d\epsilon_{ij}^p)_D$ parts as:

$$\begin{aligned} d\epsilon_{ij}^p &= (d\epsilon_{ij}^p)_V + (d\epsilon_{ij}^p)_D \\ &= d\lambda \left(\frac{\partial \phi}{\partial p} \frac{\partial p}{\partial \sigma_{ij}} + \frac{\partial \phi}{\partial q} \frac{\partial q}{\partial \sigma_{ij}} \right) \\ &= -\frac{1}{3}d\lambda \frac{\partial \phi}{\partial p} \delta_{ij} + d\lambda \frac{\partial \phi}{\partial q} n_{ij} \end{aligned} \quad (18)$$

where $\frac{\partial p}{\partial \sigma_{ij}} = -\frac{1}{3}\delta_{ij}$ and $n_{ij} = \frac{\partial q}{\partial \sigma_{ij}} = \frac{3}{2}\frac{S_{ij}}{q}$.

Substituting Eq. (18) with $-d\lambda\frac{\partial \phi}{\partial p} = d\epsilon_p$ and $d\lambda\frac{\partial \phi}{\partial q} = d\epsilon_q$, which becomes:

$$d\epsilon_{ij}^p = \frac{1}{3}d\epsilon_p\delta_{ij} + d\epsilon_q n_{ij} \quad (19)$$

where $d\epsilon_p$ and $d\epsilon_q$ are the variables corresponding to volumetric and deviatoric strain increments.

3.3. A radial return mapping algorithm

Next, the numerical integration of the constitutive relations of the model is performed using the Aravas-Zhang formulation [28, 29, 30]. Accordingly, this algorithm is based on the elastic predictor-plastic corrector, initially introduced in 1969 by Wilkins [31]. After several decades, Aravas [25] proposed a framework of the radial return algorithm by including the first invariant for the hydrostatic stress into the corrector part. Furthermore, he also provided the formulation for calculating the consistent tangent moduli (CTM). Zhang [26, 32] continued the modification by developing an explicit expression for the linearisation moduli which is close to the point return mapping algorithm. Resulting from this solution, no matrix inversion is therefore required to formulate the CTM expression.

Accordingly, this method works when a step forward in time takes the updated stress, σ_{ij}^{tr} outside the yield surface. This stress is also called trial stress or elastic predictor. The trial stress is then updated with a plastic correction to return it onto the yield surface at $t + \Delta t$ (Fig. 3) [33, 34].

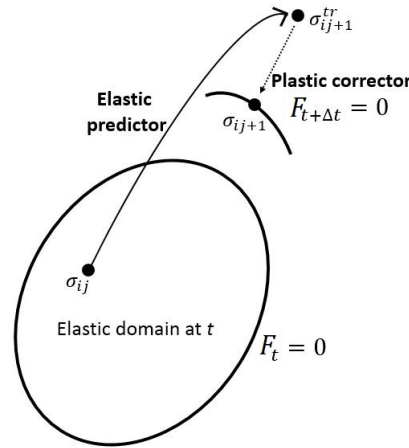


Figure 3: Geometric illustration for hardening plasticity of radial return mapping method schemes

[33, 34]

The algorithm for calculating the total strain tensor starts with:

$$\epsilon_{ij} = \epsilon_{ij}^t + \Delta\epsilon_{ij} \quad (20)$$

where $\Delta\epsilon_{ij}$ is the increment of total strain tensor. By implementing the idealized stress-strain behaviour, the relation obtained as:

$$\begin{aligned} \sigma_{ij} &= C_{ijkl}^e \epsilon_{kl}^e = C_{ijkl}^e (\epsilon_{kl} - \epsilon_{kl}^p) \\ &= C_{ijkl}^e \left[\epsilon_{kl}^t + \Delta\epsilon_{kl} - (\epsilon_{kl}^p)^t - \Delta\epsilon_{kl}^p \right] \\ &= \sigma_{ij}^{tr} - C_{ijkl}^e (\epsilon_{kl}^p) \end{aligned} \quad (21)$$

where $\epsilon_{kl} = \epsilon_{kl}^t + \Delta\epsilon_{kl}$, $\epsilon_{kl}^p = (\epsilon_{kl}^p)^t + \Delta\epsilon_{kl}^p$, $\sigma_{ij}^{tr} = C_{ijkl}^e [(\epsilon_{kl})^t + \Delta\epsilon_{kl}]$ is the trial stress and $(\epsilon_{kl}^p)^t$ is the plastic strain tensor at time step t . The term in Eq. (21) can be further elaborated as:

$$\begin{aligned} C_{ijkl}^e (\Delta\epsilon_{kl}^p) &= \left[2G\delta_{ik}\delta_{jl} + \left(K - \frac{2}{3}G \right) \delta_{ij}\delta_{kl} \right] \Delta\epsilon_{kl}^p \\ &= 2G\Delta\epsilon_{ij}^p + K\Delta\epsilon_{kk}^p\delta_{ij} - \frac{2}{3}G\Delta\epsilon_{kk}^p\delta_{ij} \end{aligned} \quad (22)$$

Substituting Eq. (19) into Eq. (22):

$$C_{ijkl}^e (\Delta\epsilon_{kl}^p) = 2G\Delta\epsilon_q n_{ij} + K\Delta\epsilon_p \delta_{ij} \quad (23)$$

Hence, Eq. (23) is used to rewrite the Eq. (21) as:

$$\sigma_{ij} = \sigma_{ij}^{tr} - 2G\Delta\epsilon_q n_{ij} - K\Delta\epsilon_p \delta_{ij} \quad (24)$$

By substituting from Eq. (16), this becomes:

$$-p\delta_{ij} + \frac{2}{3}qn_{ij} = -p^{tr}\delta_{ij} + \frac{2}{3}q^{tr}n_{ij}^{tr} - 2G\Delta\epsilon_q n_{ij} - K\Delta\epsilon_p \delta_{ij} \quad (25)$$

Thus, the correction formula for the hydrostatic pressure and equivalent stress at $t + \delta t$ can be written as:

$$p = p^{tr} + K\Delta\epsilon_p \quad (26)$$

$$q = q^{tr} - 3G\Delta\epsilon_q \quad (27)$$

3.4. Integrating the nonlinear equation

Following to the Newton Raphson method based on Taylor series expansion, $\Delta\epsilon_p$ and $\Delta\epsilon_q$ are used to formulate the internal variables of the model as [25]:

$$0 = \Delta\epsilon_p \left(\frac{\partial\phi}{\partial q} \right) + \Delta\epsilon_q \left(\frac{\partial\phi}{\partial p} \right) \quad (28)$$

$$\begin{aligned} 0 &= \Delta\epsilon_p P + \Delta\epsilon_q Q + d\Delta\epsilon_p \left[P + \Delta\epsilon_p \frac{\partial P}{\partial\Delta\epsilon_p} + \Delta\epsilon_q \frac{\partial Q}{\partial\Delta\epsilon_p} \right] \\ &+ d\Delta\epsilon_q \left[Q + \Delta\epsilon_p \frac{\partial P}{\partial\Delta\epsilon_q} + \Delta\epsilon_q \frac{\partial Q}{\partial\Delta\epsilon_q} \right] + dH^1 \left[\Delta\epsilon_p \frac{\partial P}{\partial H^1} + \Delta\epsilon_q \frac{\partial Q}{\partial H^1} \right] \\ &+ dH^2 \left[\Delta\epsilon_p \frac{\partial P}{\partial H^2} + \Delta\epsilon_q \frac{\partial Q}{\partial H^2} \right] \end{aligned} \quad (29)$$

where $P = \frac{\partial\phi}{\partial q}$ and $Q = \frac{\partial\phi}{\partial p}$, while $\partial\Delta\epsilon_p$ and $\partial\Delta\epsilon_q$ are defined as the correction values for $\Delta\epsilon_p$ and $\Delta\epsilon_q$ respectively. Moreover, the values of dH^1 and dH^2 can be determined as follows:

$$\begin{aligned} dH^1 &= -\frac{1}{\Omega} \left\{ \left(\frac{\partial G^2}{\partial H^2} \frac{\partial G^1}{\partial\Delta\epsilon_p} - \frac{\partial G^1}{\partial H^2} \frac{\partial G^2}{\partial\Delta\epsilon_p} \right) d\Delta\epsilon_p + \left(\frac{\partial G^2}{\partial H^2} \frac{\partial G^1}{\partial\Delta\epsilon_q} - \frac{\partial G^1}{\partial H^2} \frac{\partial G^2}{\partial\Delta\epsilon_q} \right) d\Delta\epsilon_q \right\} \\ &- \frac{1}{\Omega} \left\{ \left(\frac{\partial G^2}{\partial H^2} \frac{\partial G^1}{\partial p} - \frac{\partial G^1}{\partial H^2} \frac{\partial G^2}{\partial p} \right) \frac{\partial p}{\partial\Delta\epsilon_p} d\Delta\epsilon_p + \left(\frac{\partial G^2}{\partial H^2} \frac{\partial G^1}{\partial q} - \frac{\partial G^1}{\partial H^2} \frac{\partial G^2}{\partial q} \right) \frac{\partial q}{\partial\Delta\epsilon_q} d\Delta\epsilon_q \right\} \end{aligned} \quad (30)$$

$$dH^2 = -\frac{1}{\Omega} \left\{ \left(-\frac{\partial G^2}{\partial H^1} \frac{\partial G^1}{\partial \Delta \epsilon_p} + \frac{\partial G^1}{\partial H^1} \frac{\partial G^2}{\partial \Delta \epsilon_p} \right) d\Delta \epsilon_p + \left(-\frac{\partial G^2}{\partial H^1} \frac{\partial G^1}{\partial \Delta \epsilon_q} + \frac{\partial G^1}{\partial H^1} \frac{\partial G^2}{\partial \Delta \epsilon_q} \right) d\Delta \epsilon_q \right\} \\ - \frac{1}{\Omega} \left\{ \left(-\frac{\partial G^2}{\partial H^1} \frac{\partial G^1}{\partial p} + \frac{\partial G^1}{\partial H^1} \frac{\partial G^2}{\partial p} \right) \frac{\partial p}{\partial \Delta \epsilon_p} d\Delta \epsilon_p + \left(-\frac{\partial G^2}{\partial H^1} \frac{\partial G^1}{\partial q} + \frac{\partial G^1}{\partial H^1} \frac{\partial G^2}{\partial q} \right) \frac{\partial q}{\partial \Delta \epsilon_q} d\Delta \epsilon_q \right\} \quad (31)$$

where $\Omega = \left(\frac{\partial G^1}{\partial H^1} \right) \left(\frac{\partial G^2}{\partial H^2} \right) - \left(\frac{\partial G^2}{\partial H^1} \right) \left(\frac{\partial G^1}{\partial H^2} \right)$. The G^1 and G^2 are the functions made by regrouping the implicit function as:

$$G^1 = \Delta H^1 - h^1 (\Delta \epsilon_p, \Delta \epsilon_q, p, q, H^1, H^2) \quad (32)$$

$$G^2 = \Delta H^2 - h^2 (\Delta \epsilon_p, \Delta \epsilon_q, p, q, H^1, H^2) \quad (33)$$

By implementing Eq. (30) and Eq. (31) into Eq. (29) leads to the reduced form of the Newton-Raphson equation as:

$$A_{11}c_p + A_{12}c_q = b_1 \quad (34)$$

$$A_{21}c_p + A_{22}c_q = b_2 \quad (35)$$

where $d\Delta \epsilon_p = c_p$ and $d\Delta \epsilon_q = c_q$. The derivations for A_{ij} and b_i are given in Appendix A. The value of $\Delta \epsilon_p$ and $\Delta \epsilon_q$ are then updated by:

$$\Delta \epsilon_p^{n+1} = \Delta \epsilon_p^n + c_p \quad (36)$$

$$\Delta \epsilon_q^{n+1} = \Delta \epsilon_q^n + c_q \quad (37)$$

where superscript n is the iteration number.

3.5. Static implicit solution method

In this study, the implicit method has been formulated for finite element solution from static equilibrium and the solution is determined iteratively which is performed until a convergence criterion is satisfied for each increment. The virtual work principle is usually employed to explain the equilibrium state, which considers a material continuum body in volume, V and bounding surface, S subjected to surface traction, t_i and distributed body force per unit volume, f_i . The equilibrium equation can be written as [35]:

$$\int_S t_i dS + \int_V f_i dV = 0 \quad (38)$$

The Cauchy stress matrix, σ_{ij} at a point on S is defined by $t_i = \sigma_{ij}n_j$, where n_j is the unit vector outward normal to S at the point. By considering the divergence theorem of Gauss, the above equation reduces to:

$$\frac{\partial \sigma_{ij}}{\partial x_j} + f_i = 0 \quad (39)$$

Multiplying Eq. (39) by a virtual displacement, δu_i and integrating it over the whole volume, then applying the chain rule gives:

$$\int_V \sigma_{ij} \frac{\partial \delta u_i}{\partial x_j} dV - \int_S t_i \delta u_i dS - \int_V f_i \delta u_i dV = 0 \quad (40)$$

The term $\frac{\partial \delta u_i}{\partial x_j}$ is the unit relative virtual displacement, which can be decomposed into the virtual strain tensor. The equilibrium statement in Eq. (40) can be written in terms of incremental virtual displacement, $G(u_i)$ as:

$$G(u_i) = \int_V \sigma_{ij} \delta \epsilon_{ij} dV - \int_S t_i \delta u_i dS - \int_V f_i \delta u_i dV \quad (41)$$

where σ_{ij} and ϵ_{ij} are conjugate of material stress and strain measures.

If the Newton Raphson method is implemented to determine a set of solutions of Eq. (41), the estimation of the root is written as:

$$\Delta u_i^{n+1} = u_i^{n+1} - u_i^n = - \left\{ \frac{\partial G(u_i^n)}{\partial u_i} \right\}^{-1} G(u_i^n) \quad (42)$$

where superscript n is the number of iteration and $\frac{\partial G(u_i^n)}{\partial u_i}$ is the jacobian matrix of the governing equations which is presented as:

$$\frac{\partial G(u_i^n)}{\partial u_i} = K_{MN} = \int_{x^0} B_{ij,M} D_{ijkl} B_{ij,N} dV^0 + J_{MN} \quad (43)$$

where $B_{ij,M}$ and $B_{ij,N}$ are the strain variation matrices, which is based on the current position of the material point. J_{MN} is the global jacobian matrix and D_{ijkl} is the consistent tangent moduli (CTM) of the material, explained in Appendix B.

3.6. Extended Finite Element Method (XFEM)

The XFEM provides significant benefits in the numerical modelling of crack propagation where special functions are added to the finite element approximation using the partition of unity framework [15, 36]. For crack modelling, a discontinuous function also called the Heaviside step function is where the linear elastic asymptotic crack-tip displacement fields are used to account for the crack (Fig. 4). Therefore, this enables the domain to be modelled by finite elements without explicitly meshing the crack surfaces. The approximation for a displacement vector function, \mathbf{u} with the partition of unity enrichment is [18, 37]:

$$\mathbf{u} = \sum_{i=1}^n N_i(x) u_i + \sum_{i=1}^n N_i(x) H(x) a_i + \sum_{i=1}^n N_i(x) \sum_{\alpha=1}^4 F_\alpha(x) b_i^\alpha \quad (44)$$

where $N_i(x)$ is the nodal shape function, u_i is the nodal displacement vector associated with the continuous part of the finite element solution, $H(x)$ associates discontinuous jump function across the crack surfaces, a_i is the nodal enriched degree of freedom vector, $F_\alpha(x)$ represents the elastic asymptotic crack-tip functions and b_i^α is the nodal enriched degree of freedom vector. Theoretically, the first term is applicable to all nodes in the model and the second term is for nodes whose shape function support cross by the crack interior. Meanwhile, the third term is only for nodes crossing at the crack tip.

The Heaviside function, $H(x)$ across the crack surfaces gives as:

$$H(x) = \begin{cases} 1 & \text{if } \xi \geq 0 \\ -1 & \text{otherwise} \end{cases} \quad (45)$$

where $\xi = n \cdot (x - x^*)$, is the local axis perpendicular to the crack growth direction, x is a Gauss point, x^* is the point on the crack closest to x , and n is the unit outward normal to the crack at x . Moreover, the asymptotic crack tip function, $F_\alpha(x)$ is given by:

$$F_\alpha(x) = r^m \left[\sin \frac{\Theta}{2}, \cos \frac{\Theta}{2}, \sin \Theta \sin \frac{\Theta}{2}, \sin \Theta \cos \frac{\Theta}{2} \right] \quad (46)$$

where (r, Θ) is a polar coordinate system with its origin at the crack tip and m is a value which depends on the type of material. The processes flow of XFEM formulation is presented in Fig. 5. It should be noted that for XFEM elements, the location and the number of Gauss points between load increments may be changed as the crack propagates. Hence, material state variables must be updated consistently until the end of the load increment.

However, in crack propagation problems, the crack crosses over a whole element one at a time only permitting to work on plane problems with a reduced integration element, so that the stresses and strains are calculated in the centre of the element (on the integration point). Also, as the crack tip is never within an element, the singularity of the stresses does not need to be considered in the definition of the elemental displacements [39]. Moreover, the asymptotic singularity functions are only considered when modelling stationary cracks. Therefore, the crack must propagate across an entire element to avoid the need to model the stress singularity. Thus, in the crack propagation of plane problem, the XFEM discontinuous displacement approximation becomes:

$$\mathbf{u} = \sum_{i=1}^n N_i(x) u_i + \sum_{i=1}^n N_i(x) H(x) a_i \quad (47)$$

The crack initiation and direction of the crack extension need to be defined in the XFEM formulation, in order to simulate the degradation and eventual failure of an enriched element. The failure mechanism consists of two concepts: a crack initiation criterion and a damage evolution law. A crack process begins when the stresses or the strains (based on the damage of traction-separation law) satisfy specified crack initiation criteria. After that, the damage evolution law (based on displacement or energy release rate criterion) describes the rate at which the cohesive stiffness is degraded once the corresponding initiation criterion is reached.

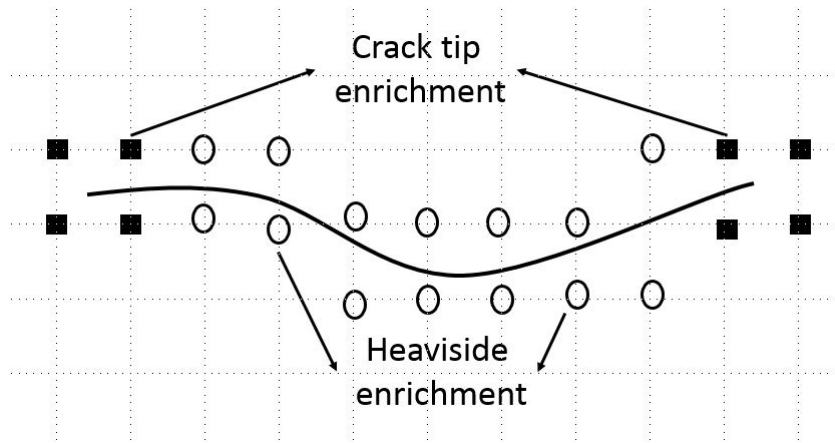


Figure 4: Enrichment nodes for the crack tip and the crack surfaces. The squared nodes (set of nodes K_{Λ}) are enriched by the crack tip functions while the circled nodes (set of nodes K_{Γ}) are enriched by the discontinuity functions

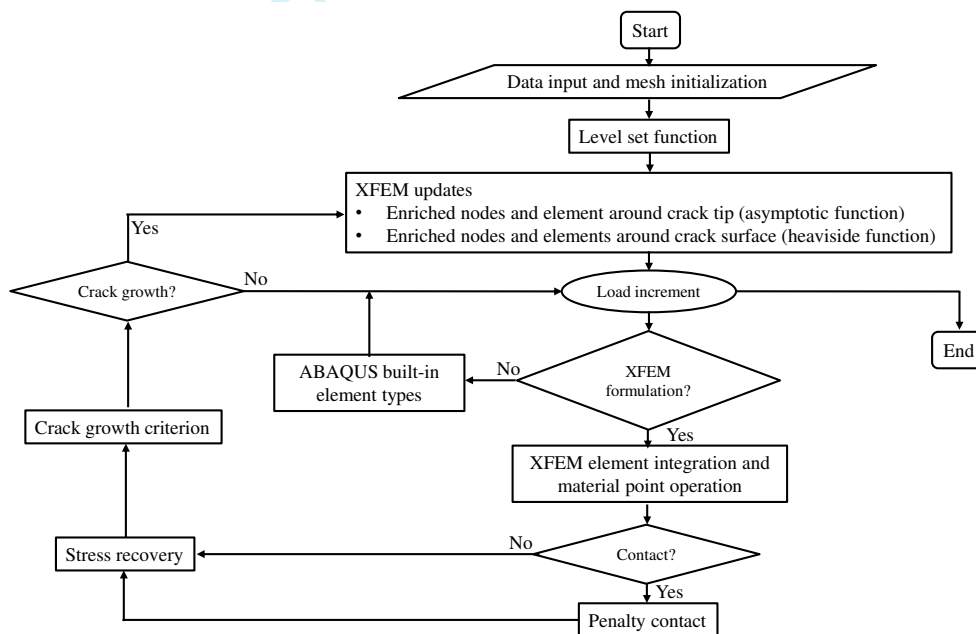


Figure 5: Flowchart of XFEM formulation [38]

4. Computational tests

4.1. Lorentz notched rod specimen

The Lorentz notched rod problem [40] is selected in this study to examine the RuX model for the void-crack assessment. The details and relevant data of A508 steel are shown in Fig. 6 and Table 1, respectively. The simulation is performed under the assumption of 2D-axial symmetry which consisting of a quadrilateral geometric element and 2484 number of nodes.

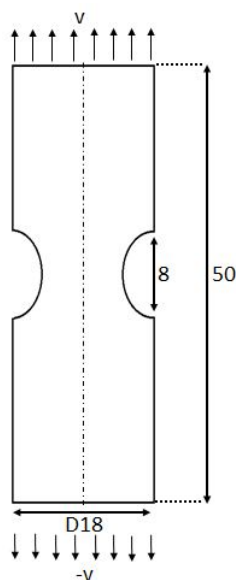


Figure 6: Geometry representation for notched tensile, A508 steel specimen

Young modulus, E	198 GPa
Poisson ratio, ν	0.3
Yield strength, σ_y	550 MPa
Rousselier parameter σ_1	490 MPa
Rousselier parameter D	2
Initial void volume fraction, f_o	0.0005

Table 1: Mechanical properties and Rousselier parameters

The distribution of the stress, void volume fraction, equivalent plastic strain and the displacement together with the crack propagation sequence are shown in Figs 7 to 10. As can be seen from the results, starting from the initiation at the center of the crack, it then propagates towards the notch until final failure. As shown in Fig. 8, the void is initiated, with growth following the direction of the crack path. The void growth which represents the damage parameter in this study shows a microscopic nature of fracture characterization. In addition, the critical value of void damage was captured, which approximately 0.00074. In the present work, it is observed, without a crack propagation, the critical void volume fraction is around 0.2. This is aligned with the significant value mentioned in literature, which is about 0.2-0.3 [23]. However, for the first time, in this paper, XFEM is combined with the Rousselier model, thus enabling the crack to propagate while keeping the observation of the void volume fraction. Hence, the energy concentration exerted by the crack is released when the crack propagated [41, 42] and resulted in a much lower void volume fraction compared to the case without crack extension. Nevertheless, the results are still can be acceptable in a purpose to predict the void damage formation with crack development.

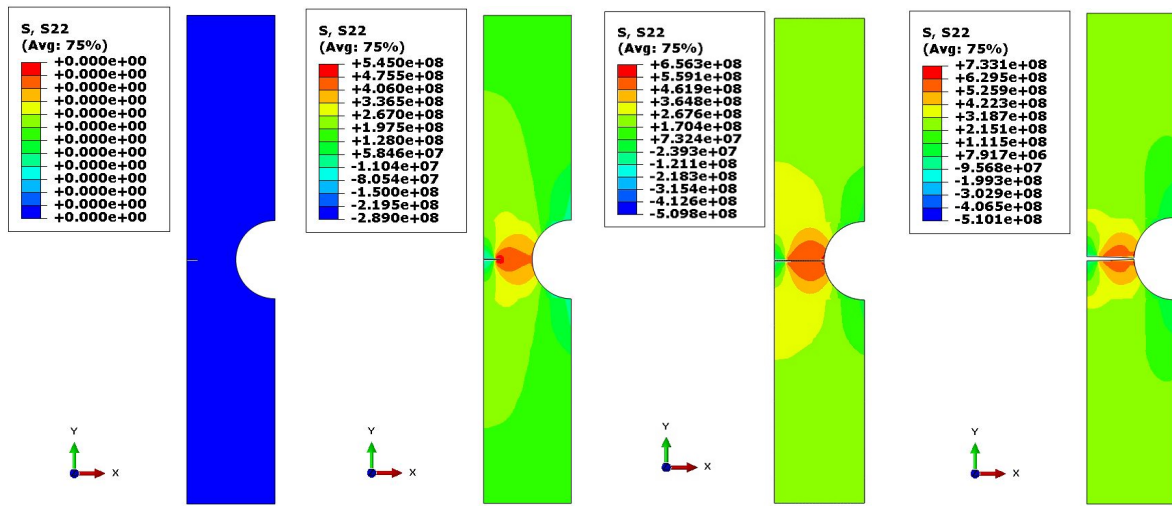


Figure 7: Stress in y-direction along the crack

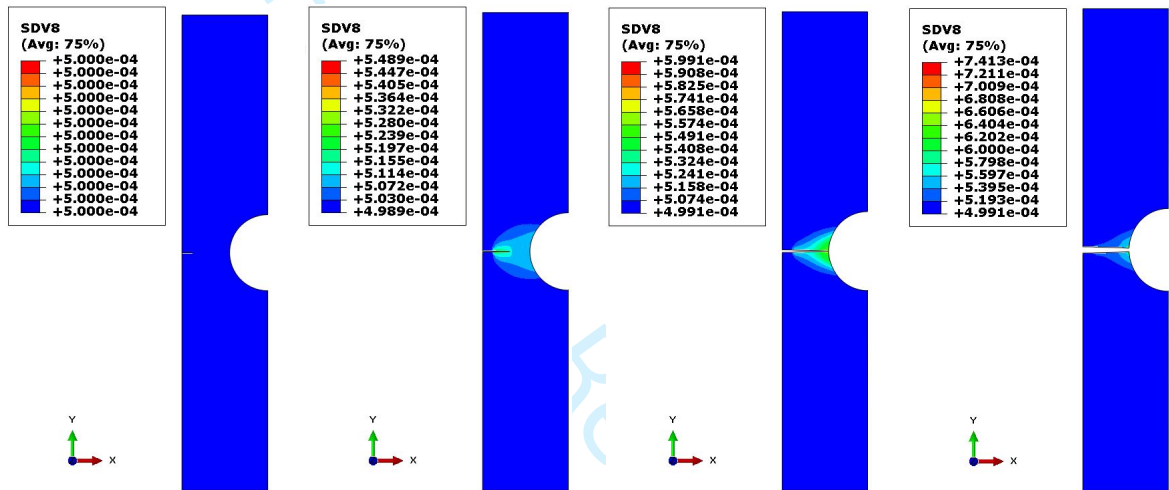


Figure 8: Void volume fraction distribution along the crack

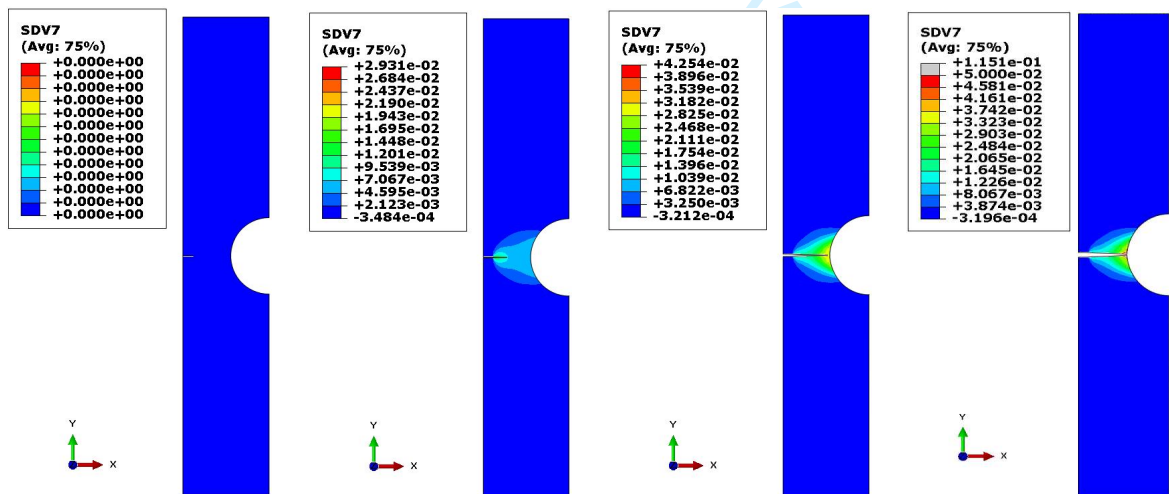


Figure 9: Equivalent plastic strain distribution along the crack

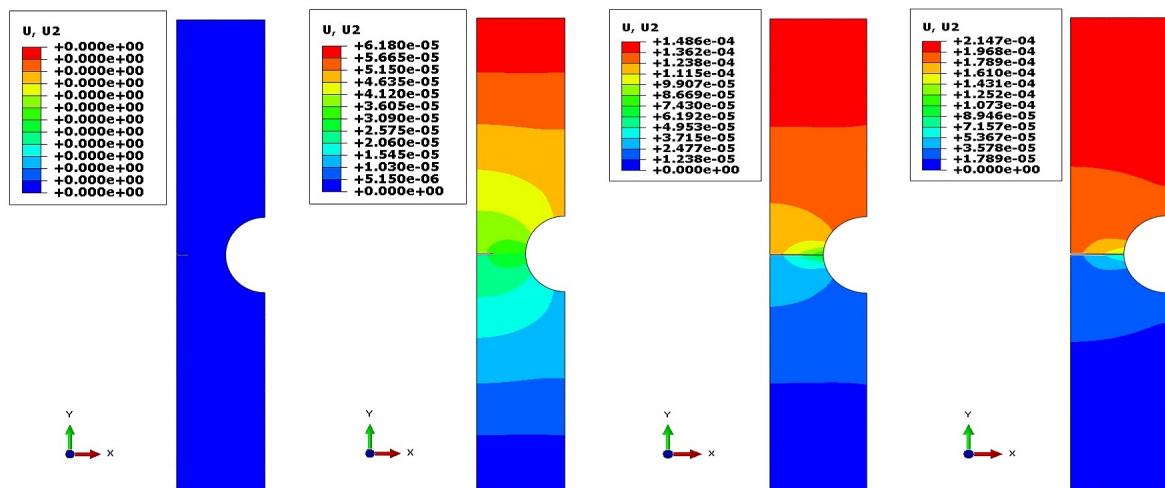


Figure 10: Displacement in y-direction distribution

Next, these results were compared with the results found in the reference [40] regarding the stress and the strain relation as shown in Fig. 11. In this figure, to trigger the connection between the damage model with the crack or its propagation, the result from XFEM is compared with the RuX model. The result shows that the XFEM formulation itself does not predict the behaviour in tension adequately. However, the result for the RuX model shows an acceptable agreement with the benchmark result from Lorentz et al. [40]. This shows that the RuX formulation connects XFEM and the damage model in an appropriate manner. As the specimen is loaded, the stress first increases because of increasing void fraction at the structural scale and then drops suddenly due to final cracks of the material. Numerical values for the similarity between the predicted and benchmark results are shown in Table 2. Similarity values of at least 95% show the effectiveness of the results in this analysis.

Table 2: Numerical values of similarity for different solution models

Solution model	Total stress, (σ_t), MPa	Similarity, %
Lorentz et al. (2008)	5957	
Rousselier	6061	98
RuX	5667	95

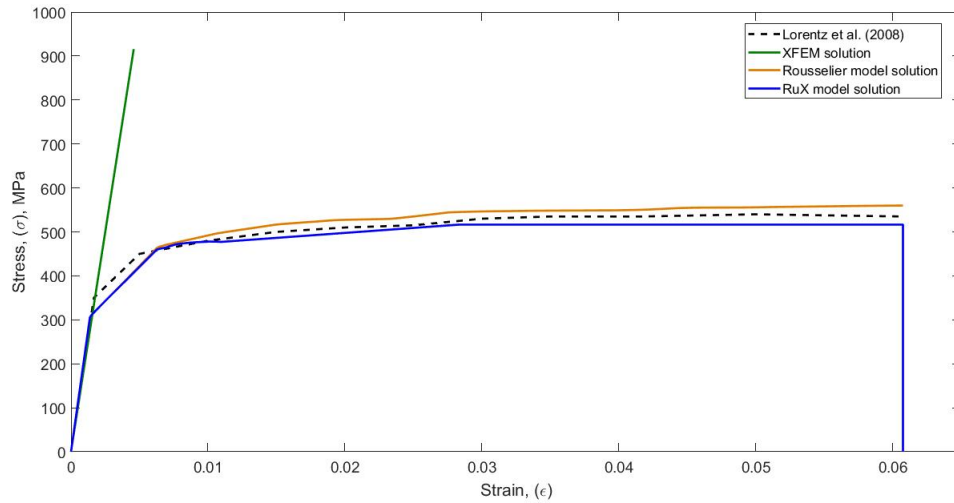


Figure 11: Stress-strain curve for notched tensile specimen

This is followed by evaluating the relation between force and displacement (Fig. 12), where the force increases with increasing displacement until it reaches final failure and then drops due to final fracture.

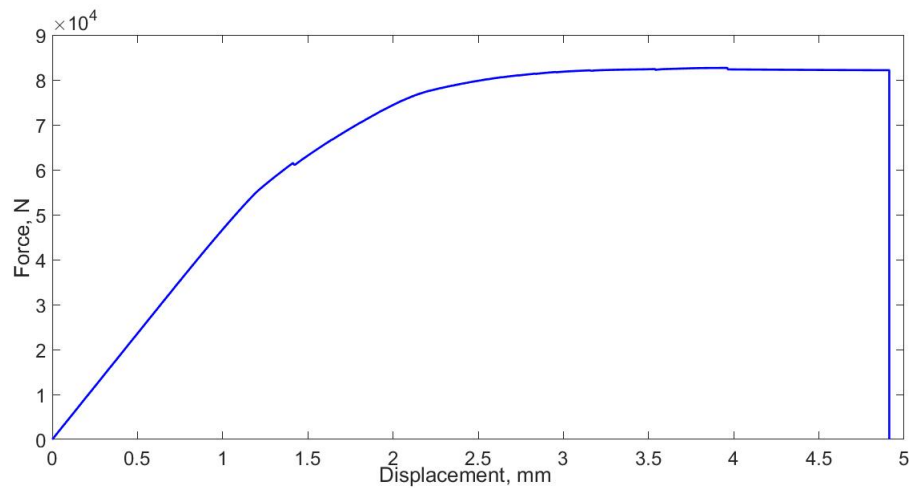


Figure 12: Force-displacement distribution

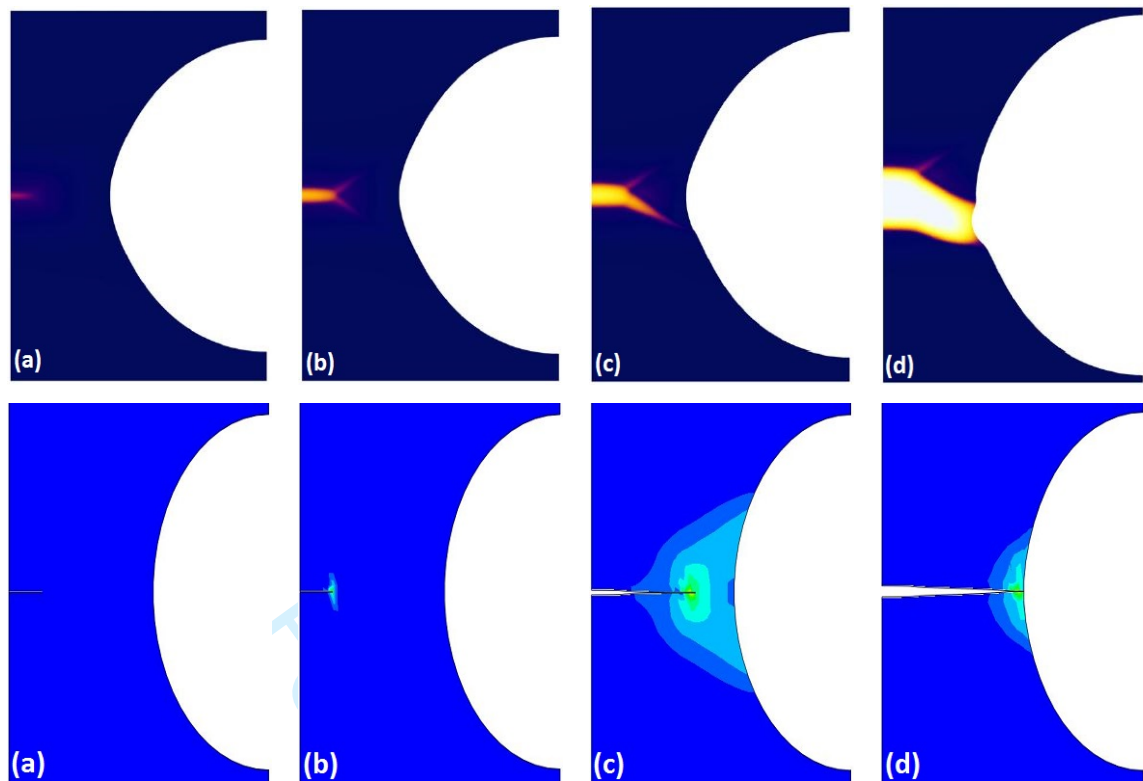


Figure 13: Evolution of damage variable in Lorentz et al. [40](above) and RuX model with crack(below)

The evolution of the void volume fraction as a damage variable between both methods is then compared to verify the predictive capability of the RuX model (Fig. 13). It should be noted that the benchmark model does not consider or predicts the actual crack development. The evolution begins when the localization phenomenon occurs due to high triaxiality in the centre of the specimen (Fig. 13(a)). The void band forms a shear band due to the influence of shear localization, and the crack initiation occurs at the crack tip based on the damage criteria of material (Fig. 13(b)). Then the evolution is extended as the voids coalesce along the shear bands and the crack propagates correspondingly, thereby resulting in the bifurcation (Fig. 13(c)). Finally, the strength of the structure is lost due to final crack or called as the ultimate fracture mode (Fig. 13(d)). Therefore, good agreement is achieved between the simulation and the benchmark results.

However, the crack propagation in the RuX model does not show signs of any formation of the bifurcation or cup-cone fracture at the plots like the results obtained from [40, 11]. There are some arguments to be highlighted at this point, which is first the crack growth direction will diverge or incline because of factors such as mesh orientation, mixed-mode loading conditions or having different material properties due to the presence of interfaces at arbitrary orientations. In this case, a standard tension test is simulated, and the material is considered homogeneous, thus it is impossible to form a cup-cone fracture behaviour in the computational results. Secondly, the crack path is influenced by the arrangement of the integration points in the elements. For this case, the crack jumps from one point to another based on the XFEM formulation, in which the enrichment functions typically consist of the near-tip asymptotic functions that capture the singularity around the crack tip and a discontinuous function that represents the jump in displacement across the crack surfaces. Note that at the crack tip, where steep gradients of

stresses and strains take place, the critical conditions for instability are achieved over some characteristic length, related to interparticle spacing. Otherwise, void coalescence and material decohesion will not occur [7].

4.1.1. Relative error and mesh convergence analysis

To validate the stability and accuracy of the simulation results, analysis of the relative error and mesh convergence was conducted. The relative error is calculated from the residuals which represent the difference between the internal and external forces acting on a model. In this case, the residual displays information that determines whether an iteration has produced an equilibrium solution [33]. If the residuals are small, the system accepts the iteration as converged. It can be seen in Fig. 14, from the readings that the maximum residual norm produced is consistent after 3000 iterations, showing that the solution achieved a stable condition and the data recorded are below the tolerance value. For this case, the tolerance is set to 0.005 and is used to determine whether a solution is converged. The tolerances must be small to provide an accurate solution but large enough to achieve the solution within a reasonable number of iterations [38]. Also, to identify the adequate size of meshing in the analysis, a mesh convergence curve is presented as shown in Fig. 15, showing the convergence and reaching a stable form [43].

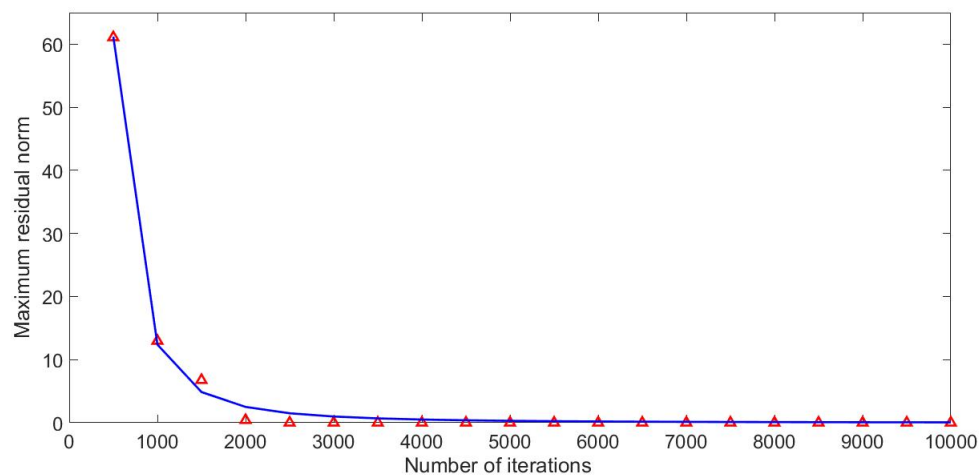


Figure 14: Maximum residual norm vs. No. of iteration

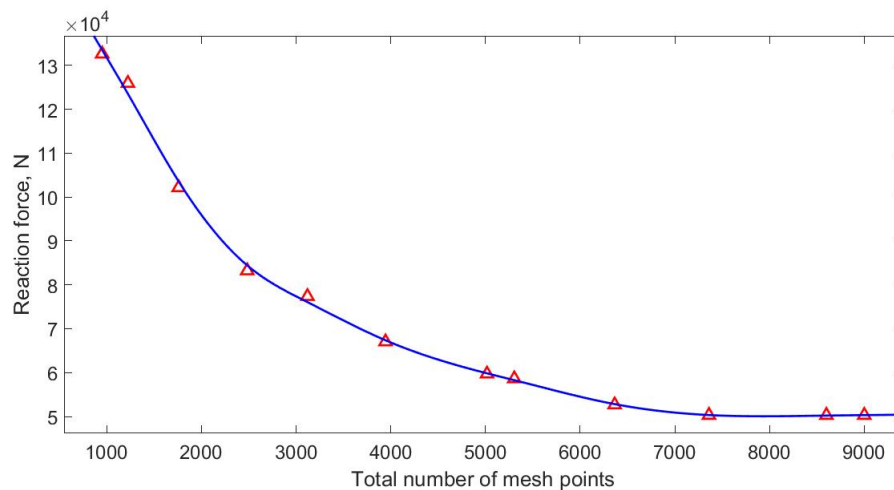


Figure 15: Mesh convergence curve

4.2. Compact tension (CT) specimen

The RuX model is further investigated using the compact tension (CT) specimen studied by Samal et al. [44]. A 2D-plane stress analysis test is performed consisting of the quadrilateral geometric element and 8398 nodes used for the specimen. The geometry and the mechanical properties of the specimen are shown in Fig. 16 and Table 3 respectively. The material of the CT specimen is low alloy steel, 22NiMoCr37 and the initial crack is 16.1 mm.

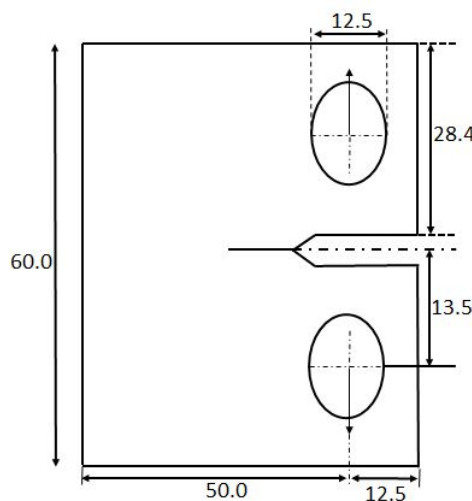


Figure 16: Geometry representation for CT-specimen

Young modulus, E	210 GPa
Poisson ratio, ν	0.3
Yield strength, σ_y	563 MPa
Rousselier parameter σ_1	445 MPa
Rousselier parameter D	2
Initial void volume fraction, f_o	0.0003

Table 3: Mechanical properties and Rousselier parameters

The contour plots for the stress and void volume fraction are shown in Figs 17 and 18. It can be observed from Fig. 18 that the highest void damage contour is concentrated at zones of high stress (as shown in Fig. 17), which is at the crack tip area. Furthermore, the contour plot of plastic potential is also presented (as shown in Fig. 19). As a final discussion point, the force, F as a function of the imposed crack mouth opening displacement, CMOD is depicted and the comparison with the experimental result is shown in Fig. 20. It can be seen that the RuX model result follows a similar trend to the experiment, with reasonable agreement. However, variances occur, especially after it enters the plastic region of material behaviour. The inability to achieve a perfect match with the experiment in this region is caused by the interaction of XFEM module in Abaqus which by default applies a linear constitutive relationship.

1
2 In contrast, the applied Rousselier model tries to follow the material's plastic behaviour. As it can be seen
3 in the previous result in Fig. 11, applying XFEM only, resulted in a linear constitutive relationship, but
4 applying the Rousselier model together fixing the result, thus, it follows the material's plastic behaviour.
5 Nevertheless, a fair performance is shown via the new algorithm, in which the crack propagation can be
6 evaluated via XFEM while it tries to maintain the plastic behaviour via the Rousselier model.
7
8
9
10
11
12
13
14
15
16
17
18
19
20
21
22
23
24
25
26
27
28
29
30
31
32
33
34
35
36
37
38
39
40
41
42
43
44
45
46
47
48
49
50
51
52
53
54
55
56
57
58
59
60

For Peer Review

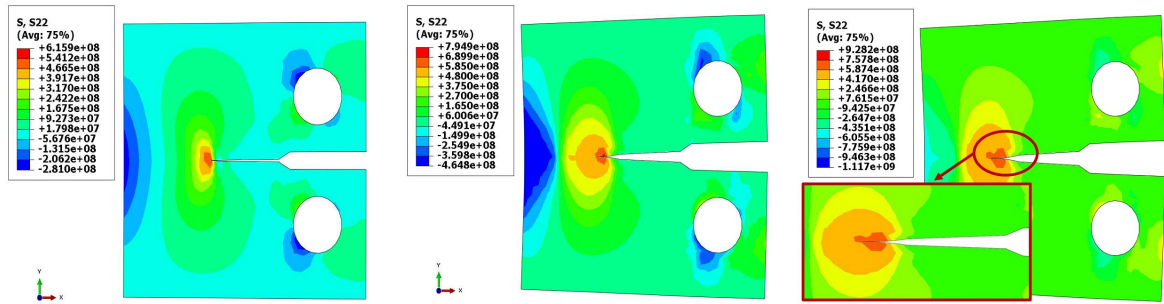


Figure 17: Stress in y-direction along the crack

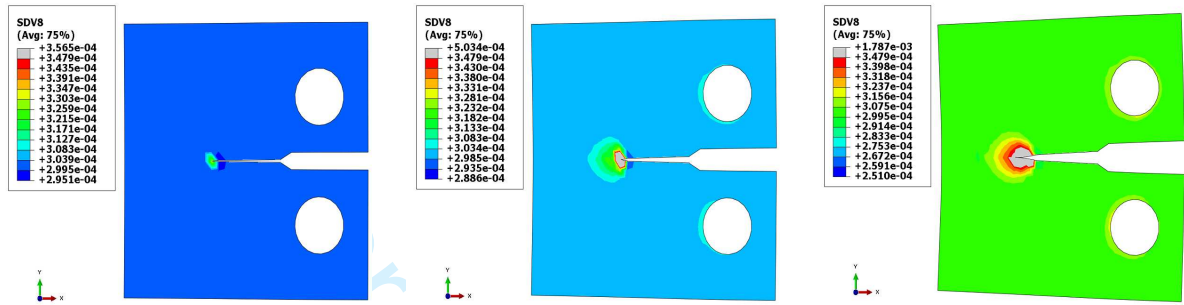


Figure 18: Void volume fraction distribution along the crack

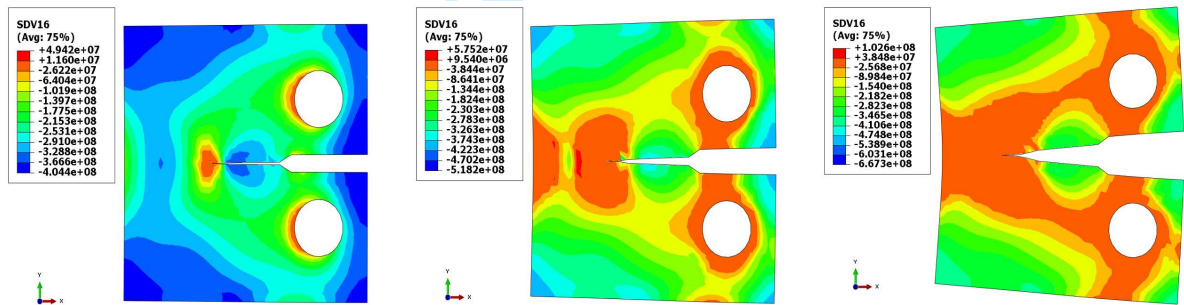


Figure 19: Plastic potential distribution along the crack

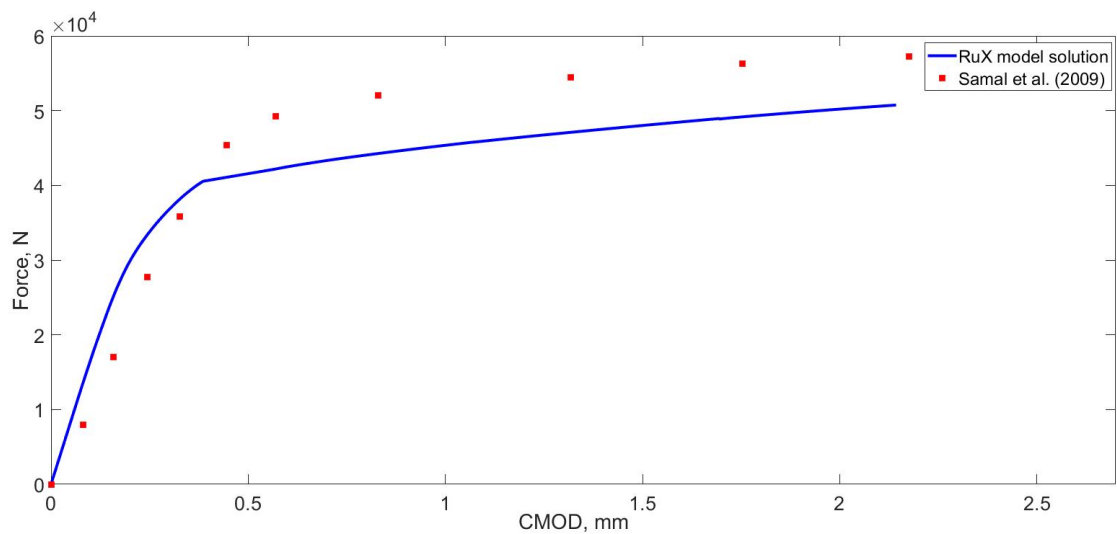


Figure 20: Force-CMOD for CT-specimen in simulation and experiment

5. Conclusion

Phenomenologically, the initiation and propagation of a crack by XFEM are investigated with the evolution of the void damage described by the Rousselier model in ductile materials. From this study, ductile fracture analysis was successfully achieved by combining the XFEM with the Rousselier damage model and the RuX model was introduced as a solution. This is the first contribution that practically describes the relationship between the void volume fraction as a damage parameter with the crack growth, which can enhance the numerical solution for the prediction of ductile fracture behaviour. There have some points that need to be highlighted here which are:

- The RuX model was tested by investigating the relation of void-crack in Lorentz-notched rod and CT-specimen. The stress-strain curve and force-displacement relation have been presented to prove that good agreement results are achieved. However, some variances need to be taken into account here due to the cause of interaction of XFEM module and the Rousselier damage model. The relative error and mesh convergence curve were presented and the overall implementation was verified.
- The evolution of the void damage using the RuX model was discussed in this study. However, the RuX model was unable to predict the bifurcation or cup-cone fracture in damage material behaviour. There are some arguments in this situation, and many factors need to be taken into account such as material properties, mesh orientation or mixed-mode loading conditions.
- The critical value of void damage formation in RuX model was relatively lower than the value obtained in previous literature. This is due to the energy concentration exerted by the crack is released when the crack propagated and resulted in a much lower void volume fraction compared to the case without crack extension. Nevertheless, the results are still acceptable in order to predict the void damage formation with crack development.

In the future study, a 3D-simulation problem will be considered and tested, to validate the capability of the developed model. In particular, attention should be paid to the convergence problems to upgrade the performance of the computational results.

6. Acknowledgements

The authors would like to express their gratitude to the University of Sheffield, the National University of Malaysia and Ministry of Education Malaysia for supporting this research project.

7. Appendix A: Coefficients in Equations 34 and 35

$$A_{11} = P + \Delta\epsilon_p \left(K \frac{\partial P}{\partial p} + \frac{\partial P}{\partial H^1} \frac{\partial H^1}{\partial \Delta\epsilon_p} + \frac{\partial P}{\partial H^2} \frac{\partial H^2}{\partial \Delta\epsilon_p} \right) + \Delta\epsilon_q \left(K \frac{\partial Q}{\partial p} + \frac{\partial Q}{\partial H^1} \frac{\partial H^1}{\partial \Delta\epsilon_p} + \frac{\partial Q}{\partial H^2} \frac{\partial H^2}{\partial \Delta\epsilon_p} \right)$$

$$A_{12} = Q + \Delta\epsilon_p \left(-3G \frac{\partial P}{\partial q} + \frac{\partial P}{\partial H^1} \frac{\partial H^1}{\partial \Delta\epsilon_q} + \frac{\partial P}{\partial H^2} \frac{\partial H^2}{\partial \Delta\epsilon_q} \right) + \Delta\epsilon_q \left(-3G \frac{\partial Q}{\partial q} + \frac{\partial Q}{\partial H^1} \frac{\partial H^1}{\partial \Delta\epsilon_q} + \frac{\partial Q}{\partial H^2} \frac{\partial H^2}{\partial \Delta\epsilon_q} \right)$$

$$A_{21} = K \frac{\partial \phi}{\partial p} + \frac{\partial \phi}{\partial H^1} \frac{\partial H^1}{\partial \Delta\epsilon_p} + \frac{\partial \phi}{\partial H^2} \frac{\partial H^2}{\partial \Delta\epsilon_p}$$

$$A_{22} = -3G \frac{\partial \phi}{\partial q} + \frac{\partial \phi}{\partial H^1} \frac{\partial H^1}{\partial \Delta \epsilon_q} + \frac{\partial \phi}{\partial H^2} \frac{\partial H^2}{\partial \Delta \epsilon_q}$$

$$b_1 = -\Delta \epsilon_p P - \Delta \epsilon_q Q$$

$$b_2 = -\phi$$

8. Appendix B: Derivation of consistence tangent modulus (CTM) formulation

To achieve convergence in the analysis, the tangent modulus formulation need to be consistent with the stress update procedure. For this study, Zhang approach [26, 45] is used which can develop an explicit CTM formula solution with the return mapping algorithm. The CTM formula is defined as:

$$D_{ijkl} = \frac{\partial \sigma_{ij}}{\partial \epsilon_{kl}} = \frac{\partial \Delta \sigma_{ij}}{\partial \Delta \epsilon_{kl}} \quad (48)$$

By referring to kinematic solution, three direct strains are defined as:

$$\partial (\epsilon_{ij})_D^{tr} = \partial (\Delta \epsilon_{ij})_D = \left(J_{ijkl} - \frac{1}{3} \delta_{ij} \delta_{kl} \right) \partial \epsilon_{kl} \quad (49)$$

$$\partial p = -K \delta_{pq} \partial \epsilon_{pq} + K \partial \Delta \epsilon_p \quad (50)$$

$$\partial \sigma_m = K \delta_{pq} \partial \epsilon_{pq} - K \partial \Delta \epsilon_p \quad (51)$$

Differentiation from Eq. (12) and using Eq. (51) gives:

$$\begin{aligned} \partial \sigma_{ij} &= K \delta_{ij} \delta_{pq} \partial \epsilon_{pq} - K \delta_{ij} \partial \Delta \epsilon_p \\ &+ \left\{ 2G \frac{q}{q^{tr}} J_{ijkl} + \frac{4G^2}{q^{tr}} \Delta \epsilon_q n_{ij} S_{ij}^{tr} \right\} \partial (\epsilon_{ij})_D^{tr} - 2G n_{ij} \partial \Delta \epsilon_q \end{aligned} \quad (52)$$

By substituting Eq. (49) into Eq. (52) as:

$$\partial \sigma_{ij} = Z_{ijkl} \partial \epsilon_{kl} - K \delta_{ij} \partial \Delta \epsilon_p - 2G n_{ij} \partial \Delta \epsilon_q \quad (53)$$

where,

$$Z_{ijkl} = \left(K - \frac{2}{3} G \frac{q}{q^{tr}} \right) \delta_{ij} \delta_{kl} + 2G \frac{q}{q^{tr}} J_{ijkl} + \frac{4G^2}{q^{tr}} \Delta \epsilon_q n_{ij} n_{kl} \quad (54)$$

By considering the linearization of the flow and yield condition at the end of the time step, the equations obtained as [26, 28]:

$$\bar{A}_{11} \partial \Delta \epsilon_p + \bar{A}_{12} \partial \Delta \epsilon_q = (B_{11} \delta_{ij} + B_{12} n_{ij}) \partial \sigma_{ij} \quad (55)$$

$$\bar{A}_{21} \partial \Delta \epsilon_p + \bar{A}_{22} \partial \Delta \epsilon_q = (B_{21} \delta_{ij} + B_{22} n_{ij}) \partial \sigma_{ij} \quad (56)$$

where the constants \bar{A}_{ij} and B_{ij} are given in Appendix C.

By substituting of Eq. (53) into Eq. (55) and Eq. (56) gives:

$$\partial\Delta\epsilon_p = (C_{11}\delta_{ij} + C_{12}n_{ij}) Z_{ijkl}\partial\epsilon_{kl} \quad (57)$$

$$\partial\Delta\epsilon_q = (C_{21}\delta_{ij} + C_{22}n_{ij}) Z_{ijkl}\partial\epsilon_{kl} \quad (58)$$

where the constants, C_{ij} are presented in Appendix D.

By substituting of Eq. (57) and Eq. (58) into Eq. (53), yields an expression of the tangent moduli consistent with the radial return method for the general pressure-dependent elastoplastic model:

$$\partial\sigma_{ij} = M_{ijkl}Z_{ijkl}\partial\epsilon_{kl} \rightarrow D_{ijkl} = \frac{\partial\sigma_{ij}}{\partial\epsilon_{kl}} = M_{ijkl}Z_{ijkl} \quad (59)$$

where,

$$M_{ijkl} = J_{ijkl} - M_{ijkl}^i - M_{ijkl}^n \quad (60)$$

$$M_{ijkl}^i = K (C_{11}\delta_{ij}\delta_{kl} + C_{12}\delta_{ij}n_{kl}) \quad (61)$$

$$M_{ijkl}^n = 2G (C_{21}n_{ij}\delta_{kl} + C_{22}n_{ij}n_{kl}) \quad (62)$$

Finally, by multiplying M_{ijkl} and Z_{ijkl} and using the relation between δ_{ij} and n_{ij} , the following explicit expression for the CTM is obtained:

$$D_{ijkl} = d_0J_{ijkl} + d_1\delta_{ij}\delta_{kl} + d_2n_{ij}n_{kl} + d_3\delta_{ij}n_{kl} + d_4n_{ij}\delta_{kl} \quad (63)$$

where the five constants are given as:

$$d_0 = 2G \frac{q}{q^{tr}} \quad (64)$$

$$d_1 = K - \frac{2G}{3} \frac{q}{q^{tr}} - 3K^2C_{11} \quad (65)$$

$$d_2 = \frac{4G^2}{q^{tr}}\Delta\epsilon_q - 4G^2C_{22} \quad (66)$$

$$d_3 = -2GKC_{12} \quad (67)$$

$$d_4 = -6GKC_{21} \quad (68)$$

it should be noted that D_{ijkl} is symmetric if $C_{12} = 3C_{21}$.

9. Appendix C: Coefficient in Equations 55 and 56

$$\bar{A}_{11} = P + \Delta\epsilon_p \left(\frac{\partial P}{\partial H^1} \frac{\partial H^1}{\partial \Delta\epsilon_p} + \frac{\partial P}{\partial H^2} \frac{\partial H^2}{\partial \Delta\epsilon_p} \right) + \Delta\epsilon_q \left(\frac{\partial Q}{\partial H^1} \frac{\partial H^1}{\partial \Delta\epsilon_p} + \frac{\partial Q}{\partial H^2} \frac{\partial H^2}{\partial \Delta\epsilon_p} \right)$$

$$\bar{A}_{21} = \frac{\partial \phi}{\partial H^1} \frac{\partial H^1}{\partial \Delta\epsilon_p} + \frac{\partial \phi}{\partial H^2} \frac{\partial H^2}{\partial \Delta\epsilon_p}$$

$$\bar{A}_{22} = \frac{\partial \phi}{\partial H^1} \frac{\partial H^1}{\partial \Delta\epsilon_q} + \frac{\partial \phi}{\partial H^2} \frac{\partial H^2}{\partial \Delta\epsilon_q}$$

$$B_{11} = \frac{\Delta\epsilon_p}{3} \left(\frac{\partial P}{\partial p} + \frac{\partial P}{\partial H^1} \frac{\partial H^1}{\partial p} + \frac{\partial P}{\partial H^2} \frac{\partial H^2}{\partial p} \right) + \frac{\Delta\epsilon_q}{3} \left(\frac{\partial Q}{\partial p} + \frac{\partial Q}{\partial H^1} \frac{\partial H^1}{\partial p} + \frac{\partial Q}{\partial H^2} \frac{\partial H^2}{\partial p} \right)$$

$$B_{12} = -\Delta\epsilon_p \left(\frac{\partial P}{\partial q} + \frac{\partial P}{\partial H^1} \frac{\partial H^1}{\partial q} + \frac{\partial P}{\partial H^2} \frac{\partial H^2}{\partial q} \right) - \Delta\epsilon_q \left(\frac{\partial Q}{\partial q} + \frac{\partial Q}{\partial H^1} \frac{\partial H^1}{\partial q} + \frac{\partial Q}{\partial H^2} \frac{\partial H^2}{\partial q} \right)$$

$$B_{21} = \frac{1}{3} \left(Q + \frac{\partial \phi}{\partial H^1} \frac{\partial H^1}{\partial p} + \frac{\partial \phi}{\partial H^2} \frac{\partial H^2}{\partial p} \right)$$

$$B_{22} = - \left(P + \frac{\partial \phi}{\partial H^1} \frac{\partial H^1}{\partial q} + \frac{\partial \phi}{\partial H^2} \frac{\partial H^2}{\partial q} \right)$$

10. Appendix D: Coefficients in Equations 61 and 62

$$C_{11} = [(\bar{A}_{22} + 3GB_{22}) B_{11} - (\bar{A}_{12} + 3GB_{12}) B_{12}] / \Delta$$

$$C_{12} = [(\bar{A}_{22} + 3GB_{22}) B_{12} - (\bar{A}_{12} + 3GB_{12}) B_{22}] / \Delta$$

$$C_{21} = [(\bar{A}_{11} + 3KB_{11}) B_{21} - (\bar{A}_{21} + 3KB_{21}) B_{11}] / \Delta$$

$$C_{22} = [(\bar{A}_{11} + 3KB_{11}) B_{22} - (\bar{A}_{21} + 3KB_{21}) B_{12}] / \Delta$$

where,

$$\Delta = (\bar{A}_{11} + 3KB_{11}) (\bar{A}_{22} + 3GB_{22}) - (\bar{A}_{12} + 3GB_{11}) (\bar{A}_{21} + 3KB_{21})$$

References

- [1] Rousselier G. and Leclercq S. (2006) *A simplified polycrystalline model for viscoplastic and damage finite element analyses*. International Journal of Plasticity 22(4):685 - 712.
- [2] Jin W. and Arson C. (2018) *Micromechanics based discrete damage model with multiple non-smooth yield surfaces: Theoretical formulation, numerical implementation and engineering applications*. International Journal of Damage Mechanics 27(5):611 - 639.
- [3] Sun D.Z, Sester M, and Schmitt W (1997) *Development and application of micromechanical material models for ductile fracture and creep damage*. International Journal of Fracture 86(1):75 - 90.
- [4] Besson J. (2010) *Continuum Models of Ductile Fracture: A Review*. International Journal of Damage Mechanics 19(1):3 - 52.

- 1
2
3
4
5
6
7
8
9
10
11
12
13
14
15
16
17
18
19
20
21
22
23
24
25
26
27
28
29
30
31
32
33
34
35
36
37
38
39
40
41
42
43
44
45
46
47
48
49
50
51
52
53
54
55
56
57
58
59
60
- [5] Gurson A.L (1977) *Continuum Theory of Ductile Rupture by Void Nucleation and Growth: Part I Yield Criteria and Flow Rules for Porous Ductile Media*. Journal of Engineering Materials and Technology 99(1):2 - 15.
- [6] Tvergaard V and Needleman A (1984) *Analysis of the cup-cone fracture in a round tensile bar*. Acta Metallurgica 32(1):157 - 169.
- [7] Rousselier G (1981) *Finite deformation constitutive relations including ductile fracture damage*. Three-dimensional constitutive relations and ductile fracture. (A 83-18477 06-39) Amsterdam, North-Holland Publishing Co. :331 - 355.
- [8] Mehdi Ganjiani (2018) *A thermodynamic consistent rate-dependent elastoplastic-damage model*. International Journal of Damage Mechanics 27(3):333 - 356.
- [9] Rousselier G, Devaux J, Motte G, and Devesa G (1977) *A Methodology for Ductile Fracture Analysis Based on Damage Mechanics: An Illustration of a Local Approach of Fracture*. STP27716S Nonlinear Fracture Mechanics: Volume II Elastic-Plastic Fracture, STP27716S, ASTM International, West Conshohocken, PA :332 - 354.
- [10] Batisse R, Bethmont M, and Devesa G, and Rousselier G (1987) *Ductile fracture of A 508 Cl 3 steel in relation with inclusion content: The benefit of the local approach of fracture and continuum damage mechanics*. Nuclear Engineering and Design 105(1):113 - 120.
- [11] Guo J, Zhao S, and Murakami R.I and Zang S. (2013) *Experimental and numerical investigation for ductile fracture of Al-alloy 5052 using modified Rousselier model*. Computational Materials Science 71:115 - 123.
- [12] Rousselier G and Luo M (2014) *A fully coupled void damage and MohrCoulomb based ductile fracture model in the framework of a Reduced Texture Methodology*. International Journal of Plasticity 55:1 - 24.
- [13] In-Bong Kim, Chol-Su Ri and Yong-Il So (2016) *A damage mechanics model of materials with voids and cracks*. International Journal of Damage Mechanics 25(6):773 - 796.
- [14] Belytschko T and Black T (1999) *Elastic crack growth in finite elements with minimal remeshing*. International Journal for Numerical Methods in Engineering 45(5):601 - 620.
- [15] Giner E, Sukumar N, Tarancn J.E and Fuenmayor F.J (2009) *An Abaqus implementation of the extended finite element method*. Engineering Fracture Mechanics 76(3):347 - 368.
- [16] Navarro-Zafra J, Curiel-Sosa J, Moreno M.S, Pinna C, Vicente J.M, Rohaizat N and Tafazolimoghaddam B (2016) *An approach for dynamic analysis of stationary cracks using XFEM*. Proceedings of the 24th UK Conference of the Association for Computational Mechanics in Engineering :303 - 308.
- [17] Curiel-Sosa J.L and Karapurath N (2012) *Delamination modelling of GLARE using the extended finite element method*. Composites Science and Technology 72(7):788 - 791.

- 1
2 [18] Sukumar N and Prvost J.H (2003) *Modeling quasi-static crack growth with the extended finite el-*
3 *ement method Part I: Computer implementation.* International Journal of Solids and Structures
4 40(26):7513 - 7537.
5
6
7 [19] Seabra M.R.R, Šuštarčić P, Cesar de Sa J.M.A and Rodič T (2013) *Damage driven crack initiation*
8 *and propagation in ductile metals using XFEM.* Computational Mechanics 52(1):161 - 179.
9
10 [20] Ruggieri C and Dotta F (2011) *Numerical modeling of ductile crack extension in high pressure*
11 *pipelines with longitudinal flaws.* Engineering Structures 33(5):1423 - 1438.
12
13 [21] Dotta F and Ruggieri C (2004) *Structural integrity assessments of high pressure pipelines with axial*
14 *flaws using a micromechanics model.* International Journal of Pressure Vessels and Piping 81(9):761
15 - 770.
16
17 [22] Seidenfuss M, Samal M.K and Roos E (2011) *On critical assessment of the use of local and nonlocal*
18 *damage models for prediction of ductile crack growth and crack path in various loading and boundary*
19 *conditions.* International Journal of Solids and Structures 48(24):3365 - 3381.
20
21 [23] Areias P, Dias-da-Costa D, Sargado J.M and Rabczuk T (2013) *Element-wise algorithm for modeling*
22 *ductile fracture with the Rousellier yield function.* Computational Mechanics 52(6):1429 - 1443.
23
24 [24] Rousellier G (1987) *Ductile fracture models and their potential in local approach of fracture.* Nuclear
25 *Engineering and Design* 105(1):97 - 111.
26
27 [25] Aravas N (1987) *On the numerical integration of a class of pressure-dependent plasticity models.*
28 *International Journal for Numerical Methods in Engineering* 24(7):1395 - 1416.
29
30 [26] Zhang Z.L (1995) *Explicit consistent tangent moduli with a return mapping algorithm for pressure-*
31 *dependent elastoplasticity models.* Computer Methods in Applied Mechanics and Engineering
32 121(1):29 - 44.
33
34 [27] Richard M. Christensen *Yield functions and plastic potentials for BCC metals and possibly other*
35 *materials.* Stanford University and Lawrence Livermore National Laboratory: 1 - 21.
36
37 [28] Zhang Z.L and Niemi E (1995) *A class of generalized mid-point algorithms for the GursonTvergaard*
38 *material model.* International Journal for Numerical Methods in Engineering 38(12):2033 - 2053.
39
40 [29] Arun S (2015) *Finite Element Modelling of Fracture and Damage in Austenitic Stainless Steel in*
41 *Nuclear Power Plant.* PhD Thesis, Faculty of Engineering and Physical Sciences, University of
42 Manchester, UK.
43
44 [30] Bensaada R, Almansba M, Ouali M.O and Hannachi, N.E (2016) *The Rousellier model implemen-*
45 *tation for a dynamic explicit analysis of the ductile fracture.* Nature & Technology (15):31.
46
47 [31] Wilkins M.L (1969) *Calculation of elastic-plastic flow.* Lawrence Radiation Laboratory, University
48 of California.
49
50 [32] Zhang Z.L (1995) *On the accuracies of numerical integration algorithms for Gurson-based pressure-*
51 *dependent elastoplastic constitutive models.* Computer Methods in Applied Mechanics and Engineer-
52 ing 121(1):15 - 28.
53
54
55
56
57
58
59
60

- 1
2 [33] Curiel-Sosa J.L, Beg O.A and Liebana Murillo J.M (2013) *Finite Element Analysis of Structural*
3 *Instability Using an Implicit/Explicit Switching Technique*. International Journal for Computational
4 Methods in Engineering Science and Mechanics 14(5):452 - 464.
5
6
7 [34] De Souza Neto E.A, Peric D. and Owen D.R.J (2008) *Computational Methods For Plasticity: Theory*
8 *and applications*. John Wiley Sons, Ltd.
9
10
11 [35] Zhang Z.L (1994) *A practical micro mechanical model based local approach methodology for the*
12 *analysis of ductile fracture of welded T-joints*. PhD Thesis, Lappeenranta University of Technology,
13 Finland.
14
15
16 [36] Wang H, Liu Z, Xu D, Zeng Q and Zhuang Z (2016) *Extended finite element method analysis*
17 *for shielding and amplification effect of a main crack interacted with a group of nearby parallel*
18 *microcracks*. International Journal of Damage Mechanics 25(1):4 - 25.
19
20
21 [37] Sukumar N, Mos N, Moran B and Belytschko T. (2000) *Extended finite element method for*
22 *three-dimensional crack modelling*. International Journal for Numerical Methods in Engineering
23 48(11):1549 - 1570.
24
25
26 [38] *Abaqus analysis user's guide documentation (2014)*. Dassault Systemes Simulia Corp. Abaqus 6,14-2.
27
28
29 [39] Serna Moreno M.C., Curiel-Sosa J.L, Navarro-Zafra J, Martinez Vicente J.L and Lopez Cela J.J
30 (2015) *Crack propagation in a chopped glass-reinforced composite under biaxial testing by means of*
31 *XFEM*. Composite Structures 119:264 - 271.
32
33
34 [40] Lorentz E, Besson J and Cano V (2008) *Numerical simulation of ductile fracture with the Rousselier*
35 *constitutive law*. Computer Methods in Applied Mechanics and Engineering 197(21):1965 - 1982.
36
37
38 [41] Curiel-Sosa J.L, Tafazzolmoghaddam B. and Zhang C (2018) *Modelling fracture and delamination*
39 *in composite laminates: Energy release rate and interface stress*. Composite Structures 189: 641 -
40 647.
41
42
43 [42] Tafazzolmoghaddam B and Curiel-Sosa J.L (2015) *On the calculation of energy release rate in*
44 *composites by finite elements, boundary elements and analytical methods*. Composites: Mechanics,
45 Computations, Applications, An International Journal 6(3): 219 - 237.
46
47
48 [43] Ahmad M.I.M, Curiel-Sosa J.L and Rongong J (2017) *Characterisation of creep behaviour using the*
49 *power law model in copper alloy*. Journal of Mechanical Engineering and Sciences 11(1):2503 - 2510.
50
51
52 [44] Samal M.K, Seidenfuss M and Roos E (2009) *A new mesh-independent Rousselier's damage model:*
53 *Finite element implementation and experimental verification*. International Journal of Mechanical
54 Sciences 51(8):619 - 630.
55
56
57 [45] Simo J.C and Taylor R.L (2014) *Consistent tangent operators for rate-independent elastoplasticity*.
58 Computer Methods in Applied Mechanics and Engineering 48(1):101 - 118.
59
60